Weakening of Tropical Free-Tropospheric Temperature Gradients with Global Warming

HENG QUAN,[a,b] YI ZHANG,[c] AND STEPHAN FUEGLISTALER[a,b]

[a] *Department of Geosciences, Princeton University, Princeton, New Jersey*
[b] *Program in Atmospheric and Oceanic Sciences, Princeton University, Princeton, New Jersey*
[c] *Courant Institute of Mathematical Sciences, New York University, New York, New York*

(Manuscript received 22 June 2024, in final form 23 September 2024, accepted 29 November 2024)

ABSTRACT: The weak temperature gradients in the tropical free troposphere due to the vanishing Coriolis force near the equator lead to a strong dynamical coupling over the entire tropics. Using theory and a suite of targeted model experiments, we show that the weak temperature gradients further weaken under global warming. We show that the temperature gradient is set by the circulation strength, with a weaker circulation being associated with weaker gradients. Thus, the known scaling difference between atmospheric radiative cooling and static stability that leads to a slowdown of the circulation under warming also leads to a weakening of the temperature gradients in the tropical free troposphere. The impact from the weakening circulation on the weakening of temperature gradients is shown to dominate over the impact of masked CO_2 forcing and the El Niño–like tropical Pacific warming pattern in model projections. Key to the result is the nonlinear zonal momentum advection term. Using the well-known Matsuno–Gill model with the correct scaling of heating and static stability may give the correct sign of the response in the temperature gradients, but inaccurate scaling, due to the linear momentum damping in that model. The robust scaling of the magnitude of the tropical quasi-stationary structure with temperature opens possibilities for theoretical advances on questions of societal relevance, ranging from changes in tropical cloudiness to heat stress under climate change.

KEYWORDS: Tropics; Nonlinear dynamics; Walker circulation; Climate change; Cloud resolving models; General circulation models

1. Introduction

Due to the small Coriolis force at low latitudes, the tropical free troposphere cannot sustain horizontal temperature gradients as large as at higher latitudes (Charney 1963). Any strong horizontal buoyancy or temperature gradients produced by deep convection would be quickly homogenized by gravity waves (Bretherton and Smolarkiewicz 1989). Consequently, on climate time scales, horizontal pressure and temperature gradients can be assumed to be small, and the "weak temperature gradient (WTG)" approximation allows to simplify the equations governing the atmospheric dynamics (Sobel and Bretherton 2000; Sobel et al. 2001).

The WTG approximation may be used to parameterize tropical planetary-scale circulation in single-column models (SCMs) and cloud-resolving models (CRMs). For example, Sobel and Bretherton (2000) proposed to parameterize the vertical velocity in SCMs in a way that represents the dominant large-scale balance between diabatic heating and vertical advection of potential temperature (Sobel et al. 2001). This approach can be generalized to CRMs (Raymond and Zeng 2005; Sessions et al. 2010; Wang and Sobel 2011; Daleu et al. 2012, 2015, 2016; Warren et al. 2020), whereby an alternative approach is the "damped gravity wave" method (Kuang 2008; Blossey et al. 2009; Romps 2012; Edman and Romps 2014).

Together with the convective quasi-equilibrium (QE) approximation [i.e., moist convection maintains the vertical temperature profile close to a moist adiabat (Arakawa and Schubert 1974; Emanuel et al. 1994)], the QE–WTG framework is the foundation to understand many aspects of tropical climate and changes therein for example due to global warming. In the QE–WTG framework, the tropical troposphere can be seen as consisting of a boundary layer with a substantial temperature gradient and a relatively homogeneous free troposphere whose temperature is determined by the subcloud moist static energy (MSE) in the regions of deep convection where subcloud MSE maximizes (e.g., Emanuel et al. 1994). This framework has been used to explain the amplified warming over land (Byrne and O'Gorman 2018), an apparent supermoist adiabatic amplification in the tropical temperature trend profile (Flannaghan and Fueglistaler 2014), the trend of tropical heat extremes (Byrne 2021; Zhang et al. 2021), the enhanced precipitation contrast between wet and dry regions with warming (Neelin et al. 2003; Chou and Neelin 2004; Zhang and Fueglistaler 2019), the ENSO teleconnections (Chiang and Sobel 2002; Lintner and Neelin 2007), the hydrological seasonal cycle in the Amazon (Anber et al. 2015), and the SST pattern effect and its impact on climate sensitivity (Ceppi and Gregory 2017; Fueglistaler 2019; Fueglistaler and Silvers 2021). Thus, the magnitude of the tropical free-tropospheric temperature gradient is of paramount importance for climate, and in the following, we address the question how global warming will affect the tropical free-tropospheric

Supplemental information related to this paper is available at the Journals Online website: https://doi.org/10.1175/JAS-D-24-0140.s1.

Corresponding author: Heng Quan, hengquan@princeton.edu

DOI: 10.1175/JAS-D-24-0140.1

temperature gradients, specifically, whether the weak temperature gradient will get weaker or stronger.

The paper is organized as follows. Section 2 provides a brief introduction to the relevant theory and mechanisms. Section 3 describes the numerical models and experiments used in this study. Section 4 tests three hypotheses regarding the weakening of the tropical free-tropospheric temperature gradients and demonstrates that the weakening of the circulation strength is fundamental. Section 5 examines the circulation weakening hypothesis using an idealized CRM in a mock Walker cell circulation, further reinforcing the hypothesis through consistency with the theoretical scaling. Finally, section 6 summarizes the results and conclusions and discusses the implications.

2. Theory

a. Background

The relation between temperature gradients, pressure gradients, and the momentum budget is discussed in Charney (1963), but how their relation responds to global warming remains incompletely understood. The atmospheric circulation is expected to slow down under global warming (Held and Soden 2006), which is based on consideration of the subsidence region where the static stability is set by remote deep convection via the WTG approximation. The radiative cooling rate increases by about 2% per kelvin warming (Jeevanjee and Romps 2018), while the static stability is linked to boundary layer humidity that scales approximately like the Clausius–Clapeyron, resulting in a weaker subsiding velocity. We want to study how the weakening of atmospheric circulation affects the temperature and pressure gradients in the tropical free troposphere.

Because of the quasi-stationary geographic structure of atmospheric latent heating in the tropics, the tropics show a pronounced quasi-stationary wave structure in the troposphere, whereby temperature gradients maximize in the upper troposphere (warm anomalies in the regions of deep convection) and around the tropical tropopause (cold anomalies over the deep convective regions), with geopotential gradients maximizing in between (e.g., Fueglistaler 2019). The model proposed by Gill (1980) provides an elegant approach to understand the tropical tropospheric quasi-stationary structure as the consequence of steady equatorial Rossby and Kelvin waves emanating from the localized heating in the regions of deep convection. The "Gill model" is widely regarded as the basis for any discussion of the large-scale structure of the tropical atmosphere and would seem the natural starting point for the problem of interest here. However, in order to arrive at an analytical solution, the Gill model represents dissipative processes as linear momentum and diabatic damping [their Eqs. (2.6)–(2.9)]. The magnitude of the momentum damping coefficient is very important as it sets the length scale of the solution, but the term is physically poorly justified and operates largely as a "tuning" parameter. Our analysis below emphasizes the importance of the momentum balance for the temperature gradient, and the Gill model may not be able to provide the insights necessary to understand the relation between circulation strength and temperature gradient. In passing, we note that a superficial look at the Gill solution may suggest an increase in the stationary wave amplitude since the latent heating term Q (precipitation) increases under global warming. The change in static stability with global warming, however, must also be considered, which is—slightly less obvious—encoded in the gravity wave phase speed $c = NH/\pi$ where stratification N is determined by static stability. Because a larger static stability decreases the stationary wave amplitude—which fights against the increase in the latent heating term Q—in a warmer climate, it is not obvious whether the stationary wave amplitude (hence free-tropospheric temperature gradients) will be larger or smaller in a warmer climate just from the Gill model.

b. Expected scaling based on the equatorial zonal momentum balance

The zonal momentum equation at a certain height $z = H$ in the free troposphere sufficiently far away from the surface is

$$\frac{\partial u}{\partial t} + \mathbf{v}\cdot\nabla u - fv = -\frac{1}{\rho}\frac{\partial p}{\partial x} + r, \tag{1}$$

where u and v are zonal and meridional velocities, $\mathbf{v}$ is the three-dimensional velocity vector, p is the pressure, and ρ is the air density. The residual term r includes unresolved processes such as the cumulus friction that was found to be important in convective regions (Lin et al. 2005; Zhou et al. 2012). The quasi-steady-state zonal pressure gradient force in the equatorial upper troposphere is primarily balanced by the zonal advection of zonal momentum [Bao et al. (2022) and our Fig. S5 in the online supplemental material]

$$u\frac{\partial u}{\partial x} \approx -\frac{1}{\rho}\frac{\partial p}{\partial x}. \tag{2}$$

In the following, we will demonstrate how the left side of Eq. (2) corresponds to the strength of the overturning circulation W, while the right side is associated with horizontal (virtual) temperature gradients δT_v in the free troposphere, linking δT_v directly to the strength of the atmospheric circulation.

The left side of Eq. (2) corresponds to the overturning circulation strength through mass conservation

$$\frac{\partial u}{\partial x} + \frac{1}{\rho}\frac{\partial(\rho w)}{\partial z} = 0, \tag{3}$$

which results in

$$\frac{U}{L} \sim \frac{W}{H}, \tag{4}$$

where L is on the scale of 10^4 km, the width of the equatorial Pacific basin. In addition, the scale of the zonal variation in u, which we denote as δU in the following, is similar to u itself, i.e., $\delta U \sim U \sim 10$ m s^{-1}. Therefore, the left side of Eq. (2) scales as

$$\frac{W^2 L}{H^2}. \tag{5}$$

The right side of Eq. (2) corresponds to zonal temperature gradients via the hydrostatic balance and the ideal gas law:

$$\ln\frac{p}{p_s} = -\frac{g}{R_d}\int_0^H \frac{dz}{T_v}, \tag{6}$$

where T_v is the height-dependent virtual temperature and p is the pressure at height $z = H$. Because we are only interested in the horizontal T_v variation, we define an effective tropospheric virtual temperature T_v^* to represent the free-tropospheric temperature as

$$T_v^* = -\frac{gH}{R_d \ln\frac{p}{p_s}}, \tag{7}$$

which is the virtual temperature of an isothermal atmosphere with the same pressure–height relation at pressure p (in the upper troposphere) as the (not isothermal) atmosphere. This simplifies the hydrostatic equation to

$$\ln\frac{p}{p_s} = -\frac{gH}{R_d T_v^*}. \tag{8}$$

Taking the zonal derivative of Eq. (8) and ignoring the zonal variation in p_s (discussions below), we get

$$\frac{\partial \ln p}{\partial x} = -\frac{gH}{R_d}\frac{\partial}{\partial x}\left(\frac{1}{T_v^*}\right), \tag{9}$$

leading to the scaling

$$\frac{\delta p}{p} \sim \frac{gH\delta T_v^*}{R_d T_v^{*2}}. \tag{10}$$

Combining this with the ideal gas law, the right side of Eq. (2) scales as

$$\frac{gH\delta T_v^*}{LT_v^*}. \tag{11}$$

We now equate the scalings in Eqs. (5) and (11) and arrive at the following scaling:

$$\frac{\delta T_v}{T_v} \sim \frac{\delta T_v^*}{T_v^*} \sim \frac{W^2L^2}{gH^3}. \tag{12}$$

This equation links the free-tropospheric temperature gradient $\delta T_v/T_v$ (which has the same scaling as $\delta T_v^*/T_v^*$, see Fig. S6) to the overturning circulation strength W, horizontal length scale L, gravitational acceleration g, and the height of the troposphere H. When we calculate the zonal derivative of Eq. (8), the surface pressure gradient is actually comparable to the upper-tropospheric pressure gradient. If we do not ignore the $\partial p_s/\partial x$ term, we would get an additional constant term in Eq. (12) that we are not interested in because $\partial p_s/\partial x$ is determined primarily by the SST gradient and independent of the circulation strength (Lindzen and Nigam 1987).

c. *The importance of the large-scale aggregation of deep convection*

The quasi-stationary structure of the tropical atmosphere reflects the large-scale distribution of deep convective heating. Any change in the geographic distribution of deep convection projects on the quasi-stationary structure and hence also on the temperature gradients in the free troposphere. The typical El Niño–like warming pattern over the tropical Pacific (according to predictions from coupled model simulations subject to anthropogenic forcings) leads to an eastward expansion of deep convection and thus to a weakening of the Walker cell and upper-tropospheric temperature gradients over the Pacific. We address the question to what extent the surface warming pattern affects the temperature gradients in the free troposphere with targeted general circulation model (GCM) experiments with prescribed SSTs.

3. Methods

a. *GCM simulations*

We use the Geophysical Fluid Dynamics Laboratory (GFDL) Forecast-Oriented Low Ocean Resolution version 2.5 of Climate Model (CM2.5-FLOR) (Vecchi et al. 2014) and its Atmosphere Model version 2.5 (AM2.5) (Delworth et al. 2012) to conduct patterned and uniform SST warming simulations. The atmosphere and land components of CM2.5-FLOR use a horizontal resolution of 0.25° × 0.25° and 32 vertical levels, and the ocean and sea ice components use a lower resolution. The greenhouse gas concentrations except CO_2 and aerosol emissions correspond to the conditions of the year 2000. We run the following experiments:

1) CM2.5-FLOR idealized CO_2 increase simulation. The CO_2 concentration starts from the observed value at the year 2000 and increases by 1% per year for 140 years (a quadrupling by the year 140). Both CO_2 concentration and SST are changing in this experiment with the coupled atmosphere–ocean GCM. Averaged fields computed from the first and last 10 years are referred to as "present climate" and "warmer climate," respectively, and their difference is the response to the CO_2 forcing.
2) Atmospheric GCM simulations with AM2.5 with prescribed SSTs from the coupled GCM experiment 1 as oceanic boundary condition. The prescribed SSTs are the mean annual cycles of the first and last 10 years of the coupled experiment 1. Both experiments are integrated for 40 years to ensure equilibration, and the last 10 years of both experiments are averaged to obtain the atmospheric GCM present climate and warmer climate states. The CO_2 concentration is fixed at the value of the year 2000. These atmospheric GCM climate states allow direct comparison with coupled GCM simulations in experiment 1 and isolate the responses to SST warming under fixed CO_2 forcing, which helps us quantify the masked CO_2 forcing effect (details below).
3) Atmospheric GCM run with prescribed SSTs from the present climate with a geographically uniform SST increase

corresponding to the global mean SST increase (approximately +3 K). This experiment is to quantify the importance of the geographic structure of the SST increase in the coupled GCM simulations. The CO_2 concentration is fixed at the value of the year 2000. Comparison of the results with the true (patterned) warming of experiment 2 allows to quantify the impact of the SST warming pattern on the tropical free-tropospheric temperature gradients.

b. CRM simulations

We use the system for atmospheric modeling (SAM; Khairoutdinov and Randall 2003), version 6.11.5, CRM for 2D (longitude/height) mock Walker simulations without rotation (similar to Kuang 2012; Wofsy and Kuang 2012). The model is nonhydrostatic, uses bulk microphysics and a simple Smagorinsky-type scheme for subgrid turbulence, and computes the surface sensible heat, latent heat, and momentum fluxes based on the Monin–Obukhov similarity theory. The vertical grid has 64 levels, starting at 25 m and extending up to 27 km, and the vertical grid spacing increases from 50 m at the lowest levels to roughly 1 km at the top of the domain. The model has a rigid lid at the top with a wave-absorbing layer occupying the upper third of the domain to prevent the reflection of gravity waves. The domain width along the x direction is $L = 10\,240$ km with a 2-km horizontal resolution, and solid wall boundary conditions are employed at the two edges.

The SSTs are prescribed and linearly decrease by 8 K from the left boundary ($x = 0$) to the right boundary ($x = 10\,240$ km), mimicking the east–west SST gradient across the equatorial Pacific. Similar to previous studies (Kuang 2012; Wofsy and Kuang 2012), we use prescribed uniform radiative cooling rates Q_{rad} throughout the troposphere (where the temperature is warmer than 207.5 K) and use a Newtonian relaxation toward 200 K in the stratosphere (Pauluis and Garner 2006). The prescribed radiative cooling allows experiments to disentangle the effects of atmospheric humidity on latent heat and static stability and on the atmospheric radiative cooling. We run two sets of simulations:

1) Simulations with fixed $Q_{\text{rad}} = -1.7$ K day^{-1} and a domain average SST ranging from 294 to 303 K with an increment of +1.5 K (i.e., 7 simulations to cover the range).
2) Simulations with the domain average SST fixed at 300 K and the radiative cooling Q_{rad} ranging from -2.9 to -0.9 K day^{-1} with an increment of 0.2 K day^{-1} (i.e., 11 simulations to cover the range).

All simulations are run for 150 days and reach equilibrium after approximately 50 days. All our results below show averaged fields computed from the last 50 days of hourly model output.

4. GCM results

Throughout this section, we analyze the virtual temperature $T_v = T(1 + 0.61q)$ (i.e., including the effect of water vapor mixing ratio on density) at the 500-hPa pressure level. We focus on zonal temperature gradients close to the equator where the Coriolis force is the smallest and the WTG approximation is most appropriate. The meridional gradients in the GCM simulations are discussed only to the extent necessary for the purpose of this paper. To avoid the additional complications due to off-equatorial latent heating particularly pronounced during the South Asian monsoon (the analytical Gill solution is based on a geographically monomodal heating distribution and does not apply to such a heating structure, rendering comparison of scalings invalid), we focus the following discussion on the results for the month of January (when the heating distribution follows much closer the idealization in Gill's analytical solution); results for the annual mean fields are similar (see Fig. S2).

a. GCM simulations show weaker temperature gradients in a warmer climate

Figure 1a shows the canonical structure (see also Bao et al. 2022) of the 500-hPa virtual temperature of the present climate, with spatial variability of order several kelvins and temperature maxima over the regions of deep convection (e.g., the equatorial western Pacific warm pool and the Amazon). The global warming simulation retains the geographic structure of the present climate, but the warming structure in Figs. 1b and 1d reveals an anticorrelation with the anomaly structure of the base state: Regions that are warmer than the average in the base state experience less than average warming and vice versa. Correspondingly, the width (Fig. 1c; quantified in terms of standard deviation) of the frequency distribution of the anomalies from the mean decreases in the "warmer climate" compared to the "present climate" simulation.

In the following, we test three possible mechanisms that could explain the decrease in the free-tropospheric temperature gradient associated with global warming: masked CO_2 forcing, changes in the geographic distribution of deep convection due to an El Niño–like SST warming pattern, and the weakening of the tropical diabatic circulation.

1) MASKED CO_2 FORCING

The first hypothesis is the masked CO_2 forcing. As pointed out by Merlis (2015), although the CO_2 concentration increase is homogeneous over the globe in global warming simulations, the radiative forcing of CO_2 is not. In the convective regions such as the western Pacific warm pool, the CO_2 radiative forcing is reduced, or "masked," compared to subsidence regions, by deep convective clouds and abundant water vapor (see also Zhang and Huang 2014). Hence, one may hypothesize that this could induce larger free-tropospheric warming in the subsiding regions (consistent with the warming pattern visible in Fig. 1b). Note that this mechanism is based on the impact on atmospheric radiative cooling and not inhomogeneous radiative forcing of the surface energy balance. To test this hypothesis, we conduct a mechanism-denial model simulation, in which we force AM2.5 (the atmosphere model of CM2.5) with the SST increase from the CM2.5-FLOR CO_2 increase simulation, but the CO_2 concentration is fixed at the value of the year 2000 (methods section). This simulation yields, compared to the reference simulation with the "masked CO_2 forcing" (Fig. 1), a similar or even stronger weakening of

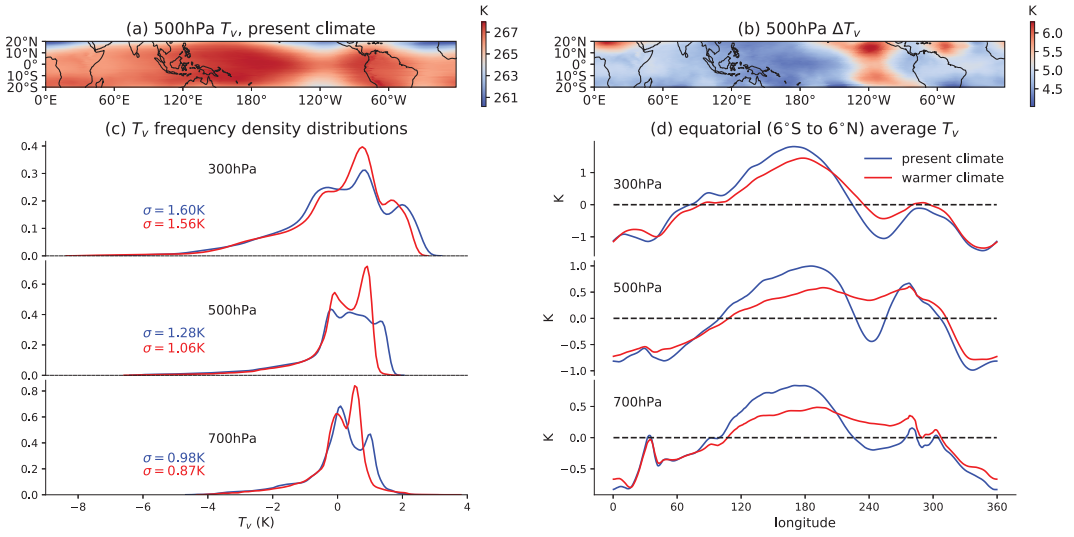

FIG. 1. Weaker temperature gradients in a warmer climate. (a) January climatological mean 500-hPa virtual temperature T_v in the present climate (years 1–10 of the CM2.5-FLOR idealized CO_2 increase simulation). (b) Response of January climatological mean 500-hPa virtual temperature ΔT_v under global warming, calculated as the difference between the warmer climate (years 131–140) and the present climate (years 1–10). (c) The frequency distributions of T_v anomalies from tropical (20°N–20°S) mean in the present climate and the warmer climate at 300-, 500-, and 700-hPa levels, with their standard deviations σ listed. (d) The zonal profiles of T_v anomalies close to the equator (meridional average between 6°N and 6°S) in the present climate and the warmer climate at 300- , 500-, and 700-hPa levels.

the temperature gradients in both the frequency distribution (Fig. 2a) and the equatorial meridional mean (Fig. 2b). Therefore, masked CO_2 forcing is not the main reason for the weaker temperature gradients in a warmer climate.

2) EL NIÑO–LIKE SST WARMING

Coupled GCM simulations yield an El Niño–like warming pattern over the tropical Pacific in the future (Dong et al. 2019). That is, the cold eastern tropical Pacific is warming more than the warm western tropical Pacific. This leads to an eastward expansion of deep convection and a weakening of the Walker cell over the tropical Pacific. Observed SST trends in recent decades do not show this warming pattern, and there is debate to what extent Walker cell strength trends are due to the weakening of the diabatic atmospheric circulation (Vecchi et al. 2006) or related to patterned SST warming and what may cause the difference in the warming pattern between coupled GCMs and observations (e.g., Po-Chedley et al. 2021). The impact of the El Niño–like warming pattern in coupled GCMs on the Walker cell—and hence also on the free-tropospheric temperature structure (see also Kamae et al. 2015)—is undisputed, and the question of interest here is whether this effect dominates, or contributes, to the weakening of the temperature gradients shown in Fig. 1.

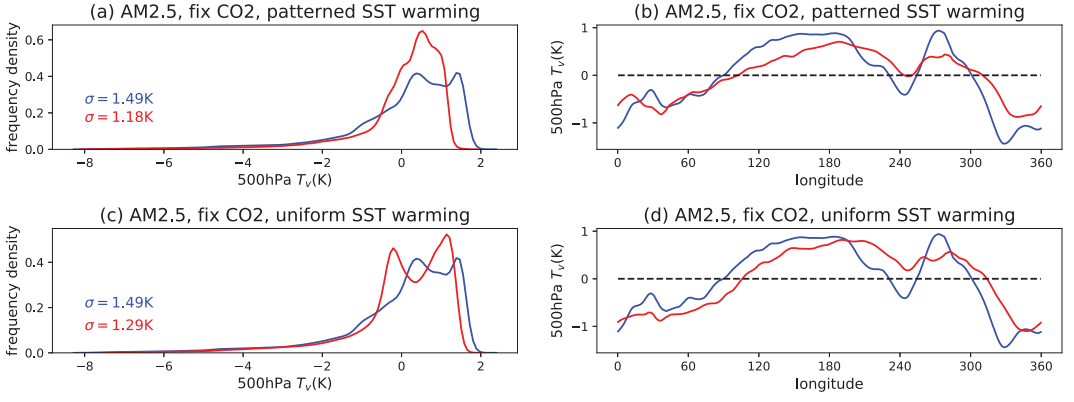

FIG. 2. Robust temperature gradient weakening across scenarios. (a),(b) As in Figs. 1c and 1d, but for AM2.5 forced by the patterned SST warming from the CM2.5-FLOR idealized CO_2 increase simulation and with fixed CO_2 concentration. (c),(d) As in Figs. 1c and 1d, but for AM2.5 forced by uniform SST warming resulting in the same global mean SST increase as the CM2.5-FLOR idealized CO_2 increase simulation and with fixed CO_2 concentration. See methods section for simulation details.

To quantify the impact of the El Niño–like warming pattern, we conduct a second mechanism-denial experiment in which we force AM2.5 with a uniform SST increase corresponding to the global mean SST warming in the CM2.5-FLOR simulation. The results of this simulation are compared to the simulation with the patterned SST change; both simulations use the same CO_2 concentration (at the value of the year 2000). This "uniform warming" simulation results in temperature gradient weakening in both frequency distribution (Fig. 2c) and equatorial zonal profile (Fig. 2d), that is smaller, but of comparable magnitude (in terms of reduction in standard deviation), to the "patterned warming" simulation. Thus, the patterned SST warming trend amplifies the weakening of the temperature gradients but is not the dominant reason for weaker temperature gradients in a warmer climate: The temperature gradients also decrease substantially under uniform warming.

3) SLOWDOWN OF THE CIRCULATION

The weaker scaling of radiative cooling compared to the scaling of the static stability under global warming implies a slowdown of the circulation (Held and Soden 2006; Vecchi and Soden 2007). This slowdown weakens the zonal momentum advection in the equatorial free troposphere and causes a corresponding weakening of the pressure gradient as required by the zonal momentum balance—which is equivalent to a weaker temperature gradient (Fig. 1d). Having shown that the masked CO_2 forcing does not lead to, and the patterned warming contributes to but is not the dominant reason for, weaker temperature gradients, we discuss the "circulation slowdown" mechanism in detail in the next section.

b. *Weaker temperature gradients attributed to weaker circulation*

To facilitate the analysis of GCM output on pressure levels, we shift to the pressure coordinate and we focus on geopotential $\Phi = gz$, as Φ and T_v are closely related if we rewrite the hydrostatic balance [Eq. (6)] in pressure coordinates as

$$\int_{p_s}^{p} -R_d T_v d\ln p = \int_0^z g dz'. \tag{13}$$

That is, the 300-hPa geopotential height z and its response under global warming Δz have an almost identical spatial pattern compared to 500-hPa virtual temperature (see Figs. S1b,d). The temperature gradient weakening in Figs. 1c and 1d is also reflected in the pressure gradient weakening in Figs. S1f and S1h. Therefore, we demonstrate that the circulation slowdown decreases the temperature gradients by showing that the circulation slowdown leads to weaker pressure gradients due to the steady-state zonal momentum balance:

$$\frac{\partial \Phi}{\partial x} = -\mathbf{v}\cdot\nabla u + fv + r, \tag{14}$$

where the four terms represent the pressure gradient force, the momentum advection, the Coriolis force, and the residual term. As before, we focus on the near-equatorial zonal structure and show the 10-yr January averages of the present and warmer climate in coupled GCM simulations. Not surprisingly, when close to the equator, the dominant balance is between the pressure gradient force and the momentum advection term (i.e., $\partial\Phi/\partial x = -\mathbf{v}\cdot\nabla u$) in both the present climate (first 10 years) and the warmer climate (last 10 years) (Figs. 3a,b), while the Coriolis force and the residual term are relatively small (Figs. 3c,d).

Following global warming, the pressure gradient force and the momentum advection term become weaker in the equatorial Pacific (Figs. 3a,b). The response of the pressure gradient $\Delta(\partial\Phi/\partial x)$ is almost equal to the response of the momentum advection $\Delta(-\mathbf{v}\cdot\nabla u)$ due to the weaker circulation (Fig. 3e), with a correlation over all longitudes of 0.91. Consistent with Bao et al. (2022), we find the reduction in the momentum advection $\Delta(-\mathbf{v}\cdot\nabla u)$ is dominated by $\Delta[-u(\partial u/\partial x)]$ (Fig. S4). The pressure gradient force and the momentum advection term only become weaker between 180° and 90°W, which is possibly due to the SST gradient response in that region associated with the El Niño–like SST warming pattern in the coupled model simulation.

Figure 3f demonstrates that both 300-hPa zonal wind and 500-hPa zonal temperature gradient become weaker under global warming, so we attribute the weaker temperature gradient to weaker momentum advection, which is a consequence of the weaker circulation. Moreover, the quadratic fit $\delta T_v \sim u^2$ achieves a smaller error than the linear fit $\delta T_v \sim u$, which is consistent with Charney (1963) and supports our argument in section 2 that temperature gradient scales with the square of circulation strength. However, these simulations do not follow the scaling $\delta T_v \sim W^2$ in Eq. (12) because the scaling $U/L \sim W/H$ is not accurate in these coupled model simulations. For a 3-K warming, W is expected to decrease by about 15% (Held and Soden 2006), while U decreases by almost 50% as shown in Fig. 3f. This is possibly due to the El Niño–ike SST warming pattern that affects the upper-tropospheric zonal wind and the response of the meridional divergence that complicates our $U/L \sim W/H$ scaling. Future work may study to what extent $U/L \sim W/H$ holds near the equator under global warming in GCM, while we will instead verify the $\delta T_v \sim W^2$ scaling in Eq. (12) by more idealized 2D CRM simulations (section 5).

Before moving on, we briefly comment on the weakening of the meridional temperature and pressure gradients, which is particularly prominent over the subtropical eastern Pacific and North Africa (Fig. 1b). In these regions, the Coriolis force is no longer negligible, and the reduction in the pressure gradient force $\Delta(-\partial\Phi/\partial y)$ in response to global warming is balanced by the reduction in the Coriolis force $\Delta(-fu)$ (Fig. S3), itself a consequence of weaker westerly wind. Future work may focus on this result and its relation to the discussion of the response of the subtropical jet to global warming (Rivière 2011; Woollings et al. 2023).

5. Theoretical scalings and CRM results

In the following, we seek theoretical understanding using a simple model, aligned with the hierarchical approach (Held 2005). As mentioned before, the linear Matsuno–Gill model would be an obvious starting point due to its ability to

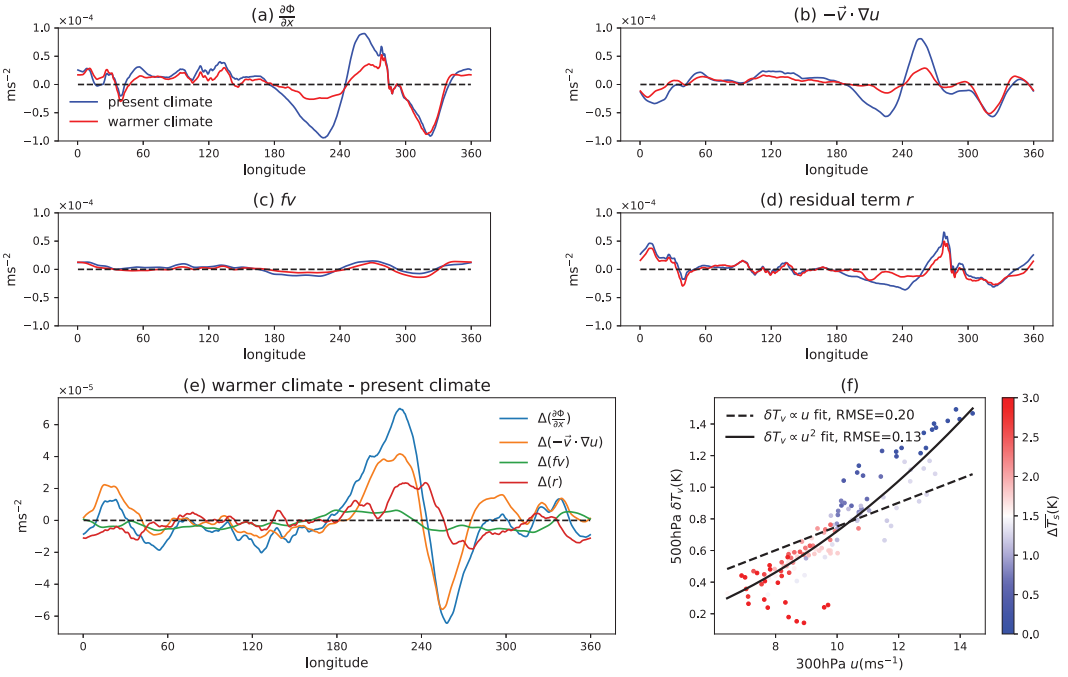

FIG. 3. (a)–(e) The 300-hPa zonal momentum budgets close to the equator (meridional average between 6°N and 6°S) for the present climate (years 1–10) and the warmer climate (years 131–140) in the CM2.5-FLOR idealized CO_2 increase simulation. (a) (minus) Pressure gradient force $\partial\Phi/\partial x$. (b) Zonal momentum advection $-\mathbf{v}\cdot\nabla u$. (c) Coriolis force fv. (d) The residual term r. (e) Responses (the warmer climate minus the present climate) of four terms to global warming. All terms are January averages in 10 years. (f) The relation between the 500-hPa virtual temperature difference between the equatorial central Pacific (meridional average between 6°N and 6°S at 180°E) and the equatorial eastern Pacific (meridional average between 6°N and 6°S at 120°W) δT_v and the mean zonal wind in this region in the 140-yr CM2.5-FLOR idealized CO_2 increase simulation. Each point is a moving average for 10 consecutive Januaries, with the color representing the increase in global mean surface temperature. The dashed/solid curves are linear/quadratic fits (both crossing the origin), and their root-mean-square errors (RMSEs) are listed.

reproduce the spatial pattern of 500-hPa ΔT_v. By converting the predicted change of convective heating (i.e., precipitation) to the forcing Q in the Gill model thermal equation [Eq. (2.8) in Gill 1980], the tropical free-tropospheric temperature gradients are weaker in a warmer climate (see Fig. 5 in Keil et al. 2023). Note that they did not adjust gravity wave phase speed (i.e., stratification) in the Gill model, which increases under global warming. Therefore, their results cannot be regarded as a "global warming" calculation. However, the explanation from the Matsuno–Gill model is quantitatively different from numerical model simulations. According to the zonal momentum equation [Eq. (2.6) in Gill 1980] in the Matsuno–Gill model, one would attribute a weaker pressure gradient $-\partial p/\partial x$ along the equator to a weaker momentum damping that is *linearly* proportional to the zonal wind, i.e., $-\epsilon u$. Below, we show that numerical model simulations instead follow the (quadratic) scaling derived in section 2.

Hence, we turn to a two-dimensional (longitude/height) numerical model simulation in order to evaluate the theoretical scaling [section 2, Eq. (12)] based on the zonal momentum equation with the dominant term $-\mathbf{v}\cdot\nabla u$. In these 2D mock Walker cell simulations, deep convection gradually becomes weaker away from the warm end and is absent in the colder part of the domain.

The numerical experiments employ uniform radiative cooling rates $Q_{\rm rad}$ throughout the troposphere and linear SST profiles as shown in Fig. 4a. This configuration is similar to the real-world equatorial Pacific and forces the majority of deep convection (and precipitation) to develop in the leftmost (warmest) 20% of the domain (Fig. 4a), resulting in a mock Walker circulation (Fig. 4b). The circulation strength is controlled by variation in the radiative cooling rate. In the limit where the steady-state thermodynamic energy equation is dominated by a balance of radiative cooling and vertical motion (typical in subsidence regions above cold SSTs), we can relate the strength of the vertical motion required by the scaling to the prescribed radiative cooling as (Lutsko and Cronin 2024)

$$w = \frac{Q_{\rm rad}}{S} = \frac{Q_{\rm rad}}{\dfrac{\partial T}{\partial z} + \dfrac{g}{c_{\rm p}}}, \tag{15}$$

where $Q_{\rm rad} < 0$ is the radiative cooling rate (K s^{-1}) and $S = (\partial T/\partial z) + (g/c_p)$ is the dry stability (K m^{-1}).

Equation (15) shows that, in addition to variations in the radiative cooling rate, the circulation strength can also be modified by variations in the static stability. As mentioned before, under global warming, both parameters change, and the

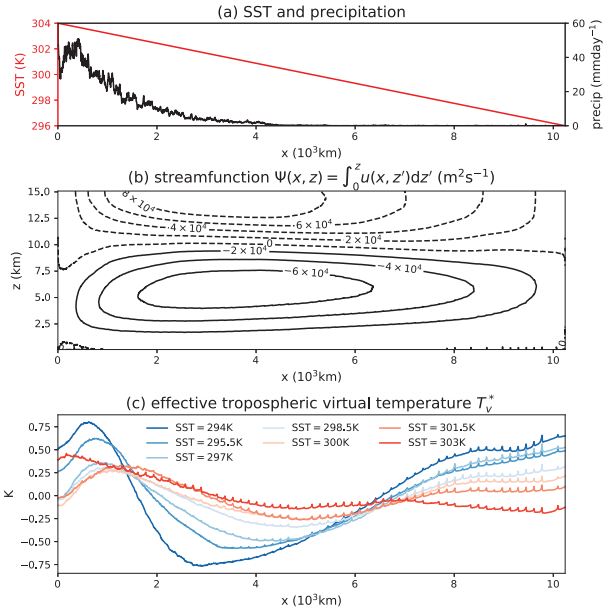

FIG. 4. (a) SST and precipitation profiles and (b) the overturning streamfunction for the simulation with $Q_{\text{rad}} = -2.1$ K day^{-1} and mean SST of 300 K. (c) The effective tropospheric virtual temperature T_v^* (details in text) anomalies (from averages along the x direction) in SAM simulations with fixed radiative cooling rate $Q_{\text{rad}} = -1.7$ K day^{-1} but different mean SSTs.

net slowdown results from the static stability scaling being larger than the radiative cooling scaling with warming. Hence, we run two sets of experiments (methods section):

1) Simulations with fixed Q_{rad} but different SSTs. Higher SSTs lead to higher subcloud specific humidity, which increases the static stability S. Hence, at fixed radiative cooling, the simulation with higher SSTs is expected to show a weaker circulation (see also appendix A, Fig. A1).
2) Simulations with fixed SSTs but different Q_{rad}. At fixed SSTs and hence fixed S, the simulation with a smaller radiative cooling rate is expected to show a weaker circulation (see also appendix A, Fig. A2).

We evaluate the horizontal gradient of the effective virtual temperature as defined in Eq. (7). For the simulations with varying radiative cooling but equal SSTs, the effective virtual temperature is evaluated for $H = 10$ km (the tropopause is at $z \approx 12$ km). For the simulations with varying SSTs but equal radiative cooling, the height level is determined as the level where the (horizontal) average temperature $\langle T \rangle = 220$ K (see appendix A for motivation and further details). Actual virtual temperatures at different levels from the $z = 5$ km level to the $z = 10$ km level show similar results as the effective tropospheric virtual temperature T_v^* (Fig. S6). Hence, the effective virtual temperature is a convenient and accurate parameter.

As expected, the CRM simulations with higher SSTs have a weaker circulation (Fig. A1a) and a weaker temperature gradient in the free troposphere (i.e., a flatter T_v^* profile in Fig. 4c). Similarly (not shown), the simulations with equal SSTs but varying radiative cooling rate show a weaker circulation and a flatter T_v^* profile for the simulations with smaller radiative cooling. Qualitatively, the 2D CRM results are consistent with the GCM results and confirm that a weaker circulation is associated with weaker temperature gradients in the free troposphere. Thus, the idealized mock Walker cell simulations can be used to quantitatively evaluate the scaling between circulation strength and temperature gradients.

The horizontal temperature gradient is expected to scale with the square of subsiding velocity W^2 all else held fixed [Eq. (12)]. Replacing W in Eq. (12) with the peak subsiding velocity w_{peak} [If we use the subsiding velocity at another level or its vertical mean value, then the proportionality coefficient in Eq. (B8) will be different, but the scaling will be the same.] in the subsiding branch (details in appendix A) gives

$$\left\langle \left| \frac{\partial T_v^*}{\partial x} \right| \right\rangle \propto w_{\text{peak}}^2, \tag{16}$$

where $\langle |\partial T_v^*/\partial x| \rangle$ is the average (absolute) horizontal T_v^* [Eq. (7)] gradient along the x direction. The proportionality coefficient in Eq. (16) is given by Eq. (B8) in appendix B.

Figure 5a shows that the theoretical relation in Eq. (16) (curves) is consistent with the model results (dots), when we change both Q_{rad} with fixed SST (blue) and SST with fixed

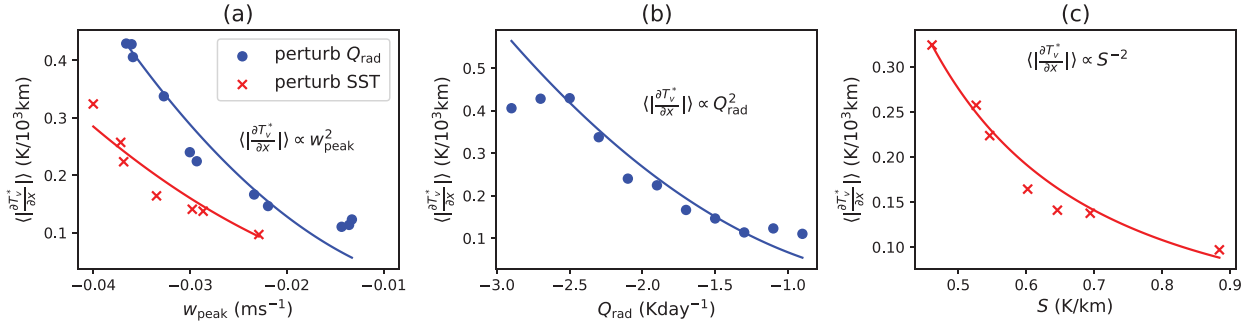

FIG. 5. Weaker circulation causes weaker temperature gradients in CRM simulations. (a) The average (absolute) horizontal T_v^* [defined in Eq. (7)] gradient along the x direction, $\langle |\partial T_v^*/\partial x| \rangle$, as a function of the peak subsiding velocity w_{peak} in the subsiding branch (details in appendix A) when we change Q_{rad} under fixed SST (blue) and change SST under fixed Q_{rad} (red). The dots are model results, and the curves are parabolas going through the origin [Eq. (B8) in appendix B]. (b) As in (a), but showing $\langle |\partial T_v^*/\partial x| \rangle$ as a function of Q_{rad} when we change Q_{rad} under fixed SST. (c) As in (a), but showing $\langle |\partial T_v^*/\partial x| \rangle$ as a function of stability S when we change SST under fixed Q_{rad}.

Q_{rad} (red). Consistent with Eq. (15), Fig. 5b shows that $\langle|\partial T_v^*/\partial x|\rangle \propto Q_{rad}^2$ when varying Q_{rad} with fixed SST, and Fig. 5c shows that $\langle|\partial T_v^*/\partial x|\rangle \propto S^{-2}$ when varying SSTs with fixed Q_{rad}. Therefore, the mock Walker cell numerical model simulations quantitatively confirm that the weaker circulation causes weaker temperature gradients in the tropical free troposphere and that the temperature gradient scales with the *square* of circulation strength (i.e., w_{peak}^2). Using the linear Matsuno–Gill model (e.g., Keil et al. 2023) to analyze the relation between circulation and temperature gradients, and how it may change under global warming, gives the result that the temperature (pressure) gradient scales *linearly* with circulation strength (i.e., U or W) because the pressure gradient force $-(1/\rho)(\partial p/\partial x)$ is balanced by the linear momentum damping term $-\alpha u$ [Eq. (2.6) in Gill 1980]. This *linear* scaling is less accurate than the *quadratic* scaling according to CRM simulations.

The equation $w = Q_{rad}/S$, as well as the argument that the circulation slows down with increasing SST or decreasing radiative cooling rate, relies on the approximation that the horizontal temperature advection $u(\partial T/\partial x)$ is much smaller than the vertical temperature advection $w(\partial T/\partial z)$. One might worry that the weakening of the temperature gradients under global warming affects the magnitude of $u(\partial T/\partial x)$ and correspondingly affects the validity of $w = Q_{rad}/S$; hence, it has a "feedback" on the slowdown of the circulation. However, since $u(\partial T/\partial x) \sim 10^{-6}$ K s$^{-1} \ll w(\partial T/\partial z) \sim 10^{-4}$ K s^{-1} and the temperature gradient $\partial T/\partial x$ does not change by order of magnitude, the equation $w = Q_{rad}/S$ is always a good approximation (as shown in Figs. A1 and A2) except for significant circulation regime shifts (discussed below). Therefore, the feedback of the weakening of temperature gradients on the slowdown of circulation can be ignored.

Finally, we note that the $\langle|\partial T_v^*/\partial x|\rangle \propto w_{peak}^2$ theory seems to hold only for a certain range of the circulation strength. Figure 5b shows that when the radiative cooling is smaller (in magnitude) than -1.5 K day^{-1} or larger (in magnitude) than -2.5 K day^{-1}, the scaling is no longer accurate. Inspection of the circulation structure (Fig. S7) shows that the simulations show a regime shift, changing from a single cell to a double cell when Q_{rad} becomes smaller (in magnitude) than -1.5 K day^{-1}. This regime shift has also been noted in similar situations by Lutsko and Cronin (2024). The scaling and its evaluation at a height of ≈10 km apply to the situation of a single overturning cell with 10 km being robustly in the upper troposphere (see appendix B). The cause for the regime shift and adapting the scaling and its evaluation to multiple cells are beyond the scope here but are important questions for future research.

6. Conclusions and outlook

Due to the smallness of the Coriolis parameter at low latitudes, the tropical free troposphere cannot maintain temperature gradients as large as at higher latitudes (Charney 1963). Using theory and a hierarchy of models, we demonstrate that horizontal temperature gradients in the tropical free troposphere will be even weaker in a warmer climate. This is because the magnitude of the temperature gradients scales with the circulation strength, and the circulation strength decreases with global warming (Held and Soden 2006; Vecchi and Soden 2007). The weaker circulation corresponds to weaker horizontal momentum advection, which then causes weaker horizontal pressure gradients in the tropical free troposphere as required by the steady-state zonal momentum equation. Due to the hydrostatic balance, the weaker pressure gradients correspond to weaker temperature gradients. This theoretical expectation is confirmed and quantitatively verified by both GCM simulations and CRM mock Walker circulation simulations shown in this paper.

Linear models such as the Matsuno–Gill model forced by predicted change of convective heating (i.e., precipitation) and stratification also yield a weakening of the temperature gradient in the free troposphere due to the weakening of the circulation. However, the scaling would be inaccurate as the Matsuno–Gill model employs a linear momentum damping, whereas in reality the zonal momentum equation is quadratic. Both the GCM simulations and the 2D mock Walker circulation model simulations confirm that the quadratic scaling is more accurate than the linear scaling.

Our results have implications for both idealized modeling and theoretical understanding of the tropical atmosphere. Parameterizations of large-scale dynamics in SCMs and CRMs need to correctly represent the weakening of the temperature gradients in simulations of global warming. Our results highlight the importance of the nonlinear momentum advection term for the understanding of changes in atmospheric dynamics with global warming and climate change in general. Direct implications of the weakening of the temperature gradient in the tropical free troposphere include processes that depend on the static stability of the lower troposphere, including heat extremes (Sherwood and Huber 2010; Zhang et al. 2021) and low cloud amount (Klein and Hartmann 1993; Ceppi and Gregory 2017; Fueglistaler 2019).

Acknowledgments. Heng Quan thanks Timothy Merlis, Zhihong Tan, and Gabriel Vecchi for helpful discussions. We thank Adam Sobel and two other anonymous reviewers for their helpful review comments. Heng Quan thanks Andrew Williams for guidance on running cloud-resolving simulations. Heng Quan thanks Wenchang Yang for providing the CM2.5 global warming simulation results. We thank Marat F. Khairoutdinov for creating and maintaining SAM. This report was prepared by Heng Quan under Award A18OAR4320123 from the National Oceanic and Atmospheric Administration, U.S. Department of Commerce. The statements, findings, conclusions, and recommendations are those of the author(s) and do not necessarily reflect the views of the National Oceanic and Atmospheric Administration, or the U.S. Department of Commerce.

Data availability statement. The model outputs and data used in this study are available upon request.

APPENDIX A

Two Ways to Vary the Strength of the Mock Walker Circulation

The circulation strength (i.e., subsidence velocity) may be modified [Eq. (15)] by either changing SSTs (to change static stability S) or changing the radiative cooling rate Q_{rad}.

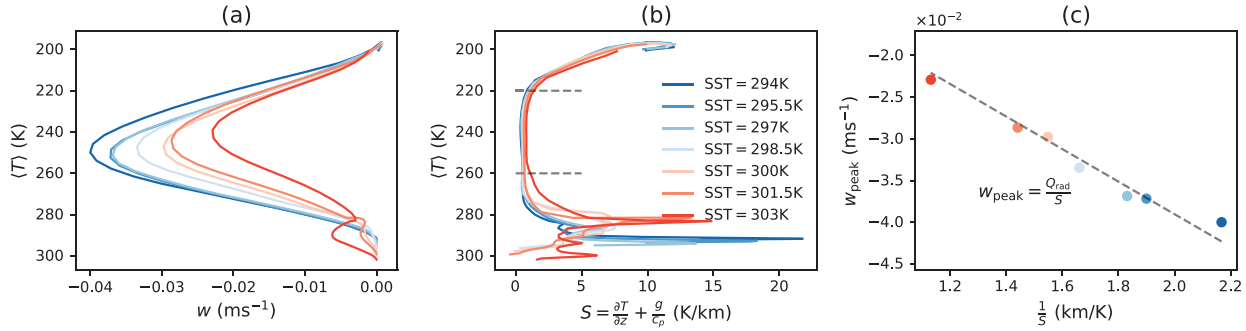

FIG. A1. Tropospheric vertical profiles of (a) vertical velocity w and (b) stability $S = (\partial T/\partial z) + (g/c_p)$ in the subsiding branch (i.e., average along the x direction above the 10% coldest SSTs) of SAM simulations with the same radiative cooling rate $Q_{\text{rad}} = -1.7$ K day^{-1} but different mean SSTs. Notice here we use temperature as the vertical coordinate. (c) The peak subsiding velocity w_{peak} as a function of $1/S$, where S is averaged between the two dotted lines in (b)—the $\langle T\rangle = 260$ K level and the $\langle T\rangle = 220$ K level. The dotted line in (c) shows their predicted relation $w_{\text{peak}} = Q_{\text{rad}}/S$ based on theory (details in text).

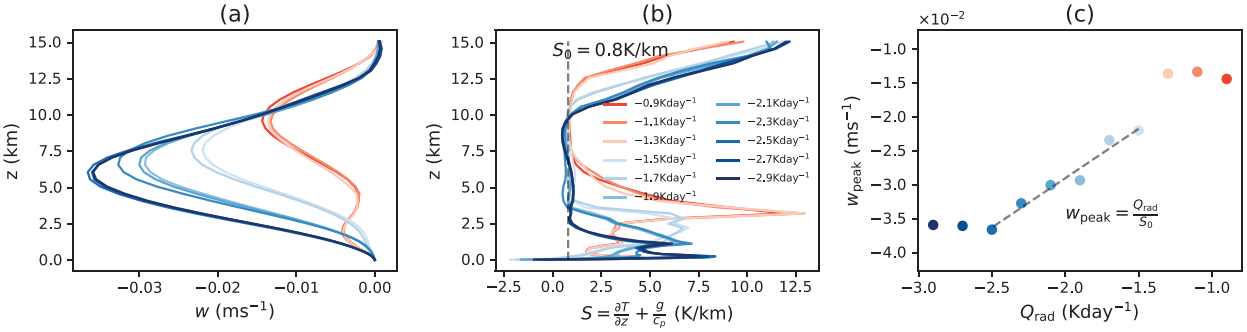

FIG. A2. Tropospheric vertical profiles of (a) vertical velocity w and (b) stability $S = (\partial T/\partial z) + (g/c_p)$ in the subsiding branch (i.e., average along the x direction above the 20% coldest SSTs) of SAM simulations with the same mean SST of 300 K but different radiative cooling rates Q_{rad}. (c) The peak subsiding velocity w_{peak} as a function of the radiative cooling rate Q_{rad}. The dotted line shows their predicted relation $w_{\text{peak}} = Q_{\text{rad}}/S_0$ based on theory (details in text), where $S_0 \approx 0.8$ K km^{-1} is the constant stability in the midtroposphere for different radiative cooling rates as marked in (b).

When increasing SSTs under fixed Q_{rad}, the subsiding velocity w indeed becomes smaller (Fig. A1a). This is because the stability $S = (\partial T/\partial z) + (g/c_p)$ in the free troposphere (vertically averaged between the $\langle T\rangle = 260$ K level and the $\langle T\rangle = 220$ K level) becomes larger in Fig. A1b. The theoretical relation $w_{\text{peak}} = Q_{\text{rad}}/S$ (line) is consistent with the model results (dots) in Fig. A1c. Note that in Figs. A1a and A1b, we follow Jeevanjee (2022) and use temperature as the vertical coordinate. This is because the circulation structure (i.e., w in Fig. A1a) remains approximately fixed in temperature coordinates, so this choice simplifies our analysis when warmer SST deepens the troposphere.

Decreasing Q_{rad} under fixed SST, the subsiding velocity w becomes smaller (Fig. A2a). In this experiment, the stability $S = (\partial T/\partial z) + (g/c_p)$ near the peak subsiding velocity in Fig. A2b has a constant value $S_0 \approx 0.8$ K km^{-1} for different radiative cooling rates. The theoretical relation $w_{\text{peak}} = Q_{\text{rad}}/S_0$ (line) is consistent with model results (dots) in Fig. A2c when Q_{rad} is between -2.5 and -1.5 K day^{-1}. When Q_{rad} is smaller (in magnitude) than -1.5 K day^{-1} or larger (in magnitude) than -2.5 K day^{-1}, however, the subsiding velocity departs from the expected scaling with the radiative cooling rate. Inspection of the mass streamfunction shows that there is a regime shift (Fig. S7) where Eq. (15) is no longer accurate.

APPENDIX B

The Theoretical Relation between Temperature Gradient and Subsiding Velocity

First, we derive how u scales with w from the continuity equation. We assume that the subsiding vertical velocity w close to the cold end of the domain $x = L$ (Figs. A1a and A2a) has the highly idealized form of

$$w = w_{\text{peak}} \sin\frac{\pi z}{H}, \tag{B1}$$

where $H = 10$ km when we change Q_{rad} under fixed SST and H is the level where $\langle T\rangle = 220$ K when we change SST under fixed Q_{rad}. We also assume the horizontal velocity u at the $z = H$ level (figure not shown) has the highly idealized form of

$$u = u_{\text{peak}} \sin\frac{\pi x}{L}, \tag{B2}$$

where the domain width $L = 10\,240$ km. Evaluating the continuity Eq. (3) [Here, we use its approximate form $(\partial u/\partial x) + (\partial w/\partial z) = 0$, which generates a ~10% error due to the $(w/\rho)(\partial\rho/\partial z)$ term but does not affect the scaling.] at $(x, z) = (L, H)$ gives

$$u_{\text{peak}} = -\frac{L}{H} w_{\text{peak}}. \tag{B3}$$

The functional forms of this idealization are applicable only to cells with length scales L and H; the regime shift to double cells violates this idealization.

Second, we derive how the pressure gradient scales with w from the momentum equation. Hourly CRM output enables us to decompose the momentum advection terms into stationary terms and eddy terms and rewrite the momentum Eq. (14) as (Yang et al. 2013)

$$-\overline{\frac{1}{\rho}\frac{\partial p}{\partial x}} + \left(-\overline{u}\frac{\partial \overline{u}}{\partial x}\right) + \left(-\overline{w}\frac{\partial \overline{u}}{\partial z}\right) + \left(-\frac{\partial \overline{u'u'}}{\partial x}\right) + \left(-\frac{\partial \overline{u'w'}}{\partial z}\right) + \overline{r} = 0, \tag{B4}$$

where $\overline{()}$ is the time average. The six terms in this equation are plotted in Figs. S5a–f for the simulation with $Q_{\text{rad}} = -2.1$ K day^{-1} and mean SST of 300 K. At the $z = H$ level in the free troposphere, the dominant balance is between the pressure gradient force and the stationary horizontal advection of horizontal momentum (Fig. S5g), so we assume

$$-\overline{\frac{1}{\rho}\frac{\partial p}{\partial x}} + \left(-\overline{u}\frac{\partial \overline{u}}{\partial x}\right) = 0. \tag{B5}$$

Utilizing Eq. (B2) for u and neglecting density variation, the pressure gradient has the form

$$\frac{\partial p}{\partial x} = -\rho u_{\text{peak}}^2 \frac{\pi}{2L} \sin\frac{2\pi x}{L}, \tag{B6}$$

so that the average (absolute) horizontal pressure gradient along the x direction is

$$\left\langle\left|\frac{\partial p}{\partial x}\right|\right\rangle = \frac{\rho}{L} u_{\text{peak}}^2 = \frac{\rho L}{H^2} w_{\text{peak}}^2. \tag{B7}$$

Finally, we derive the temperature gradient scaling with w from the hydrostatic equation. We compute the x derivative of the effective tropospheric virtual temperature T_v^* defined in Eq. (7). Neglecting the horizontal variation in p_s, we can relate $\langle|\partial T_v^*/\partial x|\rangle$ to $\langle|\partial p/\partial x|\rangle$ by

$$\left\langle\left|\frac{\partial T_v^*}{\partial x}\right|\right\rangle = \frac{gH}{R_d}\frac{1}{p(\ln p/p_s)^2}\left\langle\left|\frac{\partial p}{\partial x}\right|\right\rangle = \frac{g}{R_d}\frac{1}{p(\ln p/p_s)^2}\frac{\rho L}{H} w_{\text{peak}}^2. \tag{B8}$$

This equation tells us the coefficient in Eq. (16). Using $w_{\text{peak}} = Q_{\text{rad}}/S$, we can also get the coefficients for $\langle|\partial T_v^*/\partial x|\rangle \propto Q_{\text{rad}}^2$ and $\langle|\partial T_v^*/\partial x|\rangle \propto S^{-2}$. Figure 5 shows that the theoretical relations derived here (curves) are consistent with model results (dots). If we do not ignore the surface pressure gradient, we would have an additional constant term in Eq. (B8), which possibly makes the quadratic fitting more accurate.

REFERENCES

Anber, U., P. Gentine, S. Wang, and A. H. Sobel, 2015: Fog and rain in the Amazon. *Proc. Natl. Acad. Sci. USA*, **112**, 11 473–11 477, https://doi.org/10.1073/pnas.1505077112.

Arakawa, A., and W. H. Schubert, 1974: Interaction of a cumulus cloud ensemble with the large-scale environment, Part I. *J. Atmos. Sci.*, **31**, 674–701, https://doi.org/10.1175/1520-0469(1974)031<0674:IOACCE>2.0.CO;2.

Bao, J., V. Dixit, and S. C. Sherwood, 2022: Zonal temperature gradients in the tropical free troposphere. *J. Climate*, **35**, 7937–7948, https://doi.org/10.1175/JCLI-D-22-0145.1.

Blossey, P. N., C. S. Bretherton, and M. C. Wyant, 2009: Subtropical low cloud response to a warmer climate in a superparameterized climate model. Part II: Column modeling with a cloud resolving model. *J. Adv. Model. Earth Syst.*, **1**, 8, https://doi.org/10.3894/JAMES.2009.1.8.

Bretherton, C. S., and P. K. Smolarkiewicz, 1989: Gravity waves, compensating subsidence and detrainment around cumulus clouds. *J. Atmos. Sci.*, **46**, 740–759, https://doi.org/10.1175/1520-0469(1989)046<0740:GWCSAD>2.0.CO;2.

Byrne, M. P., 2021: Amplified warming of extreme temperatures over tropical land. *Nat. Geosci.*, **14**, 837–841, https://doi.org/10.1038/s41561-021-00828-8.

——, and P. A. O'Gorman, 2018: Trends in continental temperature and humidity directly linked to ocean warming. *Proc. Natl. Acad. Sci. USA*, **115**, 4863–4868, https://doi.org/10.1073/pnas.1722312115.

Ceppi, P., and J. M. Gregory, 2017: Relationship of tropospheric stability to climate sensitivity and Earth's observed radiation budget. *Proc. Natl. Acad. Sci. USA*, **114**, 13 126–13 131, https://doi.org/10.1073/pnas.1714308114.

Charney, J. G., 1963: A note on large-scale motions in the tropics. *J. Atmos. Sci.*, **20**, 607–609, https://doi.org/10.1175/1520-0469(1963)020<0607:ANOLSM>2.0.CO;2.

Chiang, J. C. H., and A. H. Sobel, 2002: Tropical tropospheric temperature variations caused by ENSO and their influence on the remote tropical climate. *J. Climate*, **15**, 2616–2631, https://doi.org/10.1175/1520-0442(2002)015<2616:TTTVCB>2.0.CO;2.

Chou, C., and J. D. Neelin, 2004: Mechanisms of global warming impacts on regional tropical precipitation. *J. Climate*, **17**, 2688–2701, https://doi.org/10.1175/1520-0442(2004)017<2688:MOGWIO>2.0.CO;2.

Daleu, C. L., S. J. Woolnough, and R. S. Plant, 2012: Cloud-resolving model simulations with one- and two-way couplings via the weak temperature gradient approximation. *J. Atmos. Sci.*, **69**, 3683–3699, https://doi.org/10.1175/JAS-D-12-058.1.

——, and Coauthors, 2015: Intercomparison of methods of coupling between convection and large-scale circulation: 1. Comparison over uniform surface conditions. *J. Adv. Model. Earth Syst.*, **7**, 1576–1601, https://doi.org/10.1002/2015MS000468.

——, and Coauthors, 2016: Intercomparison of methods of coupling between convection and large-scale circulation: 2. Comparison over nonuniform surface conditions. *J. Adv. Model. Earth Syst.*, **8**, 387–405, https://doi.org/10.1002/2015MS000570.

Delworth, T. L., and Coauthors, 2012: Simulated climate and climate change in the GFDL CM2.5 high-resolution coupled climate model. *J. Climate*, **25**, 2755–2781, https://doi.org/10.1175/JCLI-D-11-00316.1.

Dong, Y., C. Proistosescu, K. C. Armour, and D. S. Battisti, 2019: Attributing historical and future evolution of radiative feedbacks to regional warming patterns using a Green's function approach: The preeminence of the western Pacific. *J. Climate*, **32**, 5471–5491, https://doi.org/10.1175/JCLI-D-18-0843.1.

Edman, J. P., and D. M. Romps, 2014: An improved weak pressure gradient scheme for single-column modeling. *J. Atmos. Sci.*, **71**, 2415–2429, https://doi.org/10.1175/JAS-D-13-0327.1.

Emanuel, K. A., J. David Neelin, and C. S. Bretherton, 1994: On large-scale circulations in convecting atmospheres. *Quart. J. Roy. Meteor. Soc.*, **120**, 1111–1143, https://doi.org/10.1002/qj.49712051902.

Flannaghan, T. J., and S. Fueglistaler, 2014: Vertical mixing and the temperature and wind structure of the tropical tropopause layer. *J. Atmos. Sci.*, **71**, 1609–1622, https://doi.org/10.1175/JAS-D-13-0321.1.

Fueglistaler, S., 2019: Observational evidence for two modes of coupling between sea surface temperatures, tropospheric temperature profile, and shortwave cloud radiative effect in the tropics. *Geophys. Res. Lett.*, **46**, 9890–9898, https://doi.org/10.1029/2019GL083990.

——, and L. G. Silvers, 2021: The peculiar trajectory of global warming. *J. Geophys. Res. Atmos.*, **126**, e2020JD033629, https://doi.org/10.1029/2020JD033629.

Gill, A. E., 1980: Some simple solutions for heat-induced tropical circulation. *Quart. J. Roy. Meteor. Soc.*, **106**, 447–462, https://doi.org/10.1002/qj.49710644905.

Held, I. M., 2005: The gap between simulation and understanding in climate modeling. *Bull. Amer. Meteor. Soc.*, **86**, 1609–1614, https://doi.org/10.1175/BAMS-86-11-1609.

——, and B. J. Soden, 2006: Robust responses of the hydrological cycle to global warming. *J. Climate*, **19**, 5686–5699, https://doi.org/10.1175/JCLI3990.1.

Jeevanjee, N., 2022: Three rules for the decrease of tropical convection with global warming. *J. Adv. Model. Earth Syst.*, **14**, e2022MS003285, https://doi.org/10.1029/2022MS003285.

——, and D. M. Romps, 2018: Mean precipitation change from a deepening troposphere. *Proc. Natl. Acad. Sci. USA*, **115**, 11 465–11 470, https://doi.org/10.1073/pnas.1720683115.

Kamae, Y., H. Shiogama, M. Watanabe, M. Ishii, H. Ueda, and M. Kimoto, 2015: Recent slowdown of tropical upper tropospheric warming associated with Pacific climate variability. *Geophys. Res. Lett.*, **42**, 2995–3003, https://doi.org/10.1002/2015GL063608.

Keil, P., H. Schmidt, B. Stevens, M. P. Byrne, H. Segura, and D. Putrasahan, 2023: Tropical tropospheric warming pattern explained by shifts in convective heating in the Matsuno–Gill model. *Quart. J. Roy. Meteor. Soc.*, **149**, 2678–2695, https://doi.org/10.1002/qj.4526.

Khairoutdinov, M. F., and D. A. Randall, 2003: Cloud resolving modeling of the ARM summer 1997 IOP: Model formulation, results, uncertainties, and sensitivities. *J. Atmos. Sci.*, **60**, 607–625, https://doi.org/10.1175/1520-0469(2003)060<0607:CRMOTA>2.0.CO;2.

Klein, S. A., and D. L. Hartmann, 1993: The seasonal cycle of low stratiform clouds. *J. Climate*, **6**, 1587–1606, https://doi.org/10.1175/1520-0442(1993)006<1587:TSCOLS>2.0.CO;2.

Kuang, Z., 2008: Modeling the interaction between cumulus convection and linear gravity waves using a limited-domain cloud system–resolving model. *J. Atmos. Sci.*, **65**, 576–591, https://doi.org/10.1175/2007JAS2399.1.

——, 2012: Weakly forced mock Walker cells. *J. Atmos. Sci.*, **69**, 2759–2786, https://doi.org/10.1175/JAS-D-11-0307.1.

Lin, J.-L., M. Zhang, and B. Mapes, 2005: Zonal momentum budget of the Madden–Julian oscillation: The source and strength of equivalent linear damping. *J. Atmos. Sci.*, **62**, 2172–2188, https://doi.org/10.1175/JAS3471.1.

Lindzen, R. S., and S. Nigam, 1987: On the role of sea surface temperature gradients in forcing low-level winds and convergence in the tropics. *J. Atmos. Sci.*, **44**, 2418–2436, https://doi.org/10.1175/1520-0469(1987)044<2418:OTROSS>2.0.CO;2.

Lintner, B. R., and J. D. Neelin, 2007: A prototype for convective margin shifts. *Geophys. Res. Lett.*, **34**, L05812, https://doi.org/10.1029/2006GL027305.

Lutsko, N. J., and T. W. Cronin, 2024: The transition to double-celled circulations in mock-Walker simulations. *Geophys. Res. Lett.*, **51**, e2024GL108945, https://doi.org/10.1029/2024GL108945.

Merlis, T. M., 2015: Direct weakening of tropical circulations from masked CO_2 radiative forcing. *Proc. Natl. Acad. Sci. USA*, **112**, 13 167–13 171, https://doi.org/10.1073/pnas.1508268112.

Neelin, J. D., C. Chou, and H. Su, 2003: Tropical drought regions in global warming and El Niño teleconnections. *Geophys. Res. Lett.*, **30**, 2275, https://doi.org/10.1029/2003GL018625.

Pauluis, O., and S. Garner, 2006: Sensitivity of radiative–convective equilibrium simulations to horizontal resolution. *J. Atmos. Sci.*, **63**, 1910–1923, https://doi.org/10.1175/JAS3705.1.

Po-Chedley, S., B. D. Santer, S. Fueglistaler, M. D. Zelinka, P. J. Cameron-Smith, J. F. Painter, and Q. Fu, 2021: Natural variability contributes to model–satellite differences in tropical tropospheric warming. *Proc. Natl. Acad. Sci. USA*, **118**, e2020962118, https://doi.org/10.1073/pnas.2020962118.

Raymond, D. J., and X. Zeng, 2005: Modelling tropical atmospheric convection in the context of the weak temperature gradient approximation. *Quart. J. Roy. Meteor. Soc.*, **131**, 1301–1320, https://doi.org/10.1256/qj.03.97.

Rivière, G., 2011: A dynamical interpretation of the poleward shift of the jet streams in global warming scenarios. *J. Atmos. Sci.*, **68**, 1253–1272, https://doi.org/10.1175/2011JAS3641.1.

Romps, D. M., 2012: Weak pressure gradient approximation and its analytical solutions. *J. Atmos. Sci.*, **69**, 2835–2845, https://doi.org/10.1175/JAS-D-11-0336.1.

Sessions, S. L., S. Sugaya, D. J. Raymond, and A. H. Sobel, 2010: Multiple equilibria in a cloud-resolving model using the weak temperature gradient approximation. *J. Geophys. Res.*, **115**, D12110, https://doi.org/10.1029/2009JD013376.

Sherwood, S. C., and M. Huber, 2010: An adaptability limit to climate change due to heat stress. *Proc. Natl. Acad. Sci. USA*, **107**, 9552–9555, https://doi.org/10.1073/pnas.0913352107.

Sobel, A. H., and C. S. Bretherton, 2000: Modeling tropical precipitation in a single column. *J. Climate*, **13**, 4378–4392, https://doi.org/10.1175/1520-0442(2000)013<4378:MTPIAS>2.0.CO;2.

——, J. Nilsson, and L. M. Polvani, 2001: The weak temperature gradient approximation and balanced tropical moisture waves. *J. Atmos. Sci.*, **58**, 3650–3665, https://doi.org/10.1175/1520-0469(2001)058<3650:TWTGAA>2.0.CO;2.

Vecchi, G. A., and B. J. Soden, 2007: Global warming and the weakening of the tropical circulation. *J. Climate*, **20**, 4316–4340, https://doi.org/10.1175/JCLI4258.1.

——, ——, A. T. Wittenberg, I. M. Held, A. Leetmaa, and M. J. Harrison, 2006: Weakening of tropical Pacific atmospheric

circulation due to anthropogenic forcing. *Nature*, **441**, 73–76, https://doi.org/10.1038/nature04744.

——, and Coauthors, 2014: On the seasonal forecasting of regional tropical cyclone activity. *J. Climate*, **27**, 7994–8016, https://doi.org/10.1175/JCLI-D-14-00158.1.

Wang, S., and A. H. Sobel, 2011: Response of convection to relative sea surface temperature: Cloud-resolving simulations in two and three dimensions. *J. Geophys. Res.*, **116**, D11119, https://doi.org/10.1029/2010JD015347.

Warren, R. A., M. S. Singh, and C. Jakob, 2020: Simulations of radiative-convective-dynamical equilibrium. *J. Adv. Model. Earth Syst.*, **12**, e2019MS001734, https://doi.org/10.1029/2019MS001734.

Wofsy, J., and Z. Kuang, 2012: Cloud-resolving model simulations and a simple model of an idealized Walker cell. *J. Climate*, **25**, 8090–8107, https://doi.org/10.1175/JCLI-D-11-00692.1.

Woollings, T., M. Drouard, C. H. O'Reilly, D. M. Sexton, and C. McSweeney, 2023: Trends in the atmospheric jet streams are emerging in observations and could be linked to tropical warming. *Commun. Earth Environ.*, **4**, 125, https://doi.org/10.1038/s43247-023-00792-8.

Yang, W., R. Seager, and M. A. Cane, 2013: Zonal momentum balance in the tropical atmospheric circulation during the global monsoon mature months. *J. Atmos. Sci.*, **70**, 583–599, https://doi.org/10.1175/JAS-D-12-0140.1.

Zhang, M., and Y. Huang, 2014: Radiative forcing of quadrupling CO_2. *J. Climate*, **27**, 2496–2508, https://doi.org/10.1175/JCLI-D-13-00535.1.

Zhang, Y., and S. Fueglistaler, 2019: Mechanism for increasing tropical rainfall unevenness with global warming. *Geophys. Res. Lett.*, **46**, 14 836–14 843, https://doi.org/10.1029/2019GL086058.

——, I. Held, and S. Fueglistaler, 2021: Projections of tropical heat stress constrained by atmospheric dynamics. *Nat. Geosci.*, **14**, 133–137, https://doi.org/10.1038/s41561-021-00695-3.

Zhou, L., A. H. Sobel, and R. Murtugudde, 2012: Kinetic energy budget for the Madden–Julian oscillation in a multiscale framework. *J. Climate*, **25**, 5386–5403, https://doi.org/10.1175/JCLI-D-11-00339.1.